Effect of an α-Methyl Substituent on the Dienophile on Diels-Alder *endo*:*exo* Selectivity

Olatz Larrañaga[a] and Abel de Cózar*[a, b]

A detailed computational study of the Diels-Alder reaction of cyclopentadiene with acrylonitrile, methylacrylate and their α-methylated counterparts methacrylonitrile and methyl methacrylate at the M06-2X(PCM)/TZVP level of theory has been performed. We want to understand the excellent *exo*-selectivities observed experimentally due the presence of this substituent. To this end, analysis of the reaction coordinate by means of activation strain model of chemical reactivity (ASM-distortion interaction model) including solvation effects and NBO second order perturbation energy have been carried out.

1. Introduction

The Diels-Alder [4 + 2] cycloaddition is the most useful chemical reaction to form six-member rings. Its relevance relies on that it can potentially create up to four stereocenters regioselectively and stereospecifically in a single synthetic step. Due to that, a tremendous amount of theoretical work has been devoted to the analysis of the reaction mechanism trying to understand the excellent *endo*:*exo* selectivity observed experimentally.[1] The most accepted rationalization for the empirical *endo* rule formulated by Alder and Stein ("maximum accumulation of double bonds")[2] was proposed by Hoffmann and Woodward[3] by using orbital symmetry relationships and correlation diagrams. The authors proposed the existence of attractive secondary orbital interactions (SOI) between p orbitals not directly involved in the formation of the new sigma bonds as underlying reason for such selectivity. Although SOI has been invoked to explain preference of *endo's* cycloadduct formation,[4] even in textbooks, its existence has been criticized over the years[5] and the debate is still open.

In the early 2000s, Cossío et al.[6] studied the archetypal reaction of cyclopentadiene (**1**) and maleic anhydride (**2**) that selectively leads to *endo* cycloadduct formation (Scheme 1).[7] The authors analyzed the HOMO (**1**)-LUMO (**2**) two-electron interaction applying second-order perturbation theory.[8] In addition, they computed the second–order energy of localized

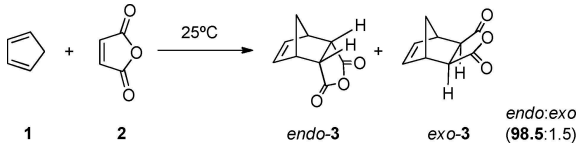

Scheme 1. Diels-Alder reaction of cyclopentadiene (**1**) and maleic anhydride (**2**). *Endo*:*exo* selectivity value taken from Ref. [7].

1 C–C π-bonding and **2** C–O π*-antibonding orbitals by means of NBO[9] calculations. The authors conclude that "SOI do exist and are responsible for at least an important part of the observed stereocontrol" and "despite SOI absolute magnitude being small, cannot be discarded a priori" (Scheme 1).

A few years later, Svatos et al.[10] performed a experimental-theoretical study of the cycloaddition reaction of cyclopentadiene (**1**) and furan (**4**) with maleic anhydride (**2**) or maleimide (**5**). The authors claim that "SOI is of limited use in explaining the observed trends in the title reactions," thus maintaining the debate.

In 2014, Fernández and Bickelhaupt[11] reevaluated the **1** + **2** reaction by using the activation strain model (ASM, also known as distortion / interaction model)[12] in combination with the energy decomposition analysis (EDA).[13] The authors found that "the interaction term[14] appears to be not at all decisive for the endo selectivity." They proposed the increase of strain energy in the *exo* pathway due to the movement of the methylene unit away from the oxygen atoms (compared to the *endo* approach) as the main responsible for the *endo*-preference instead. Thus, dismounting the orbital interaction-based explanation for the *endo* rule. This same reaction was analyzed by Sakata et al.[15] more recently. In this case, the authors propose that the electrostatic attractions derived from the presence of highly polarized C–O bonds are the responsible of the *endo*-preference, and not the orbital interactions.

However, despite the huge amount of effort devoted to the analysis of archetypal reactions, in comparison, the number of theoretical works dealing with the effect of (aliphatic) substituents on the reactivity-selectivity of Diels-Alder cycloadditions is scarce.[16] The most recent studies are focused on the reaction of substituted cyclopropenes with butadiene, showing the

[a] *Dr. O. Larrañaga, Dr. A. de Cózar*
Departamento de Química Orgánica I
Facultad de Química
Universidad del País Vasco and Donostia International Physics Center (DIPC)
P. K. 1072, E-20018, San Sebastián-Donostia (Spain)
E-mail: abel.decozar@ehu.eus
[b] *Dr. A. de Cózar*
IKERBASQUE
Basque Foundation for Science
E-48013, Bilbao (Spain)

relevance electrostatic interactions[5c] as well as SOI and charge transfer interactions.[17]

Remarkably, Houk et al.[18] computationally analyzed reactions of 5-substituted of cyclopentadienes with maleic anhydride (**2**). The authors described a correlation between the hyperconjugative aromaticity of the substituted cyclopentadienes and the activation barriers, showing that stabilization through hyperconjugative interactions within the 5–member ring reduces the reactivity by increasing the energy required to deform this fragment, but no evaluation of the *endo*:*exo* selectivities were addressed.

Contrarily, the number of experimental studies focused on the effect of substitution on the *endo*:*exo* selectivities of Diels-Alder reactions is higher.[19] In our opinion, one of the most surprising results was described by Furukawa et al.[20] (Scheme 2). The authors studied the reaction of cyclopentadiene (**1**) with acrylonitrile (**6a**), methylacrylate (**7a**) and their α-methylated counterparts methacrylonitrile (**6b**) and methyl methacrylate (**7b**) as dienophiles, realizing that the presence of methyl group in α–position to the electron-withdrawing group induces a greater tendency towards formation of *exo* cycloadducts (Scheme 2).

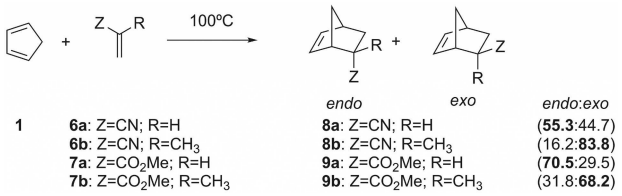

Scheme 2. Diels-Alder reaction of cyclopentadiene (**1**) and dienophiles **6–7**. *Endo*:*exo* selectivity values taken from Ref. [20].

The calculations here presented are focused on the analysis of the Diels-Alder cycloadditions [4 + 2] of cyclopentadiene (**1**) and dienophiles **6–7** collected in Scheme 2. The key questions considered are: Is this change in the selectivity merely consequence of sterical reasons? What is the relevance of SOI? and does any other σ-π interaction between reagents (namely hyperconjugation) play any effect on it? Thus, the purpose of this work is trying to shed light on the reasons of the drastic change in the *endo*:*exo* selectivity of Diels-Alder [4 + 2] cycloadditions due to the presence of a methyl group in α-position to the electron-withdrawing group. To this end, a detailed theoretical analysis on the reaction profiles within the DFT framework analysis has been performed. The trends in reactivity were further analyzed by means of the activation strain model of chemical reactivity (ASM–distortion/interaction model) and second order perturbation energy within NBO scheme.

2. Results and Discussion

First, we started exploring all the stationary points along the reaction coordinate associated with the Diels-Alder cycloaddition of cyclopentadiene (**1**) and dienophiles **6–7**. Activation and reaction Gibbs free energies as well as the main geometrical features of the transition structures computed at the M06-2X (PCM)/TZVP level of theory are shown in Table 1 and Figure 1, respectively. Relative energies were computed using the least energetic reactive complex as reference in order to avoid energetic errors derived from using standard solvated states.

Our results show that the initial reaction complex evolves through a concerted but slightly asynchronous[21] transition structure towards formation of the energetically favored cycloadduct in all the studied reactions. Moreover, the computed *endo*:*exo* selectivities are in good agreement with the experimental results of Furukawa et al.[20]

In all cases, the presence of a methyl group in α-position of the dienophile implies an increase in the computed activation barrier. However, that effect is higher in the *endo* approach than in the *exo* one. For instance, an increase of 3.55 kcal mol^{-1} is observed for *endo* approach of nitrile derivatives **6a**–**6b**, where as in the *exo* approach, the difference is of only of 2.24 kcal mol^{-1}. As a consequence, methylated compounds **6**–**7b** show a higher preference toward *exo*-cycloadducts formation than their unmethylated counterparts **6**–**7a**.

Inspection the transition structure geometries show that d_{1a} distances are shorter than their d_{4b} counterparts, as a consequence of the higher reactivity of the β-position in these asymmetric dienophiles. In addition, in most cases, the asynchronicity is also enhanced by the presence of a methyl group in α-position. Therefore, our calculations show that the methyl substituent have effect both in the energetic profiles and in the geometry of the transition structures.

In order to gain a deeper understanding of the effect of the α-methyl substituent, we performed an activation strain (ASM) – distortion/interaction analysis[12] of the reaction profiles. The obtained activation strain diagrams (ASDs) are shown in Figure 2. Decomposition of the strain energy in their fragments is shown in Figure 3 and the EDA of the interaction curve is shown in Figure 4.

The ASD obtained for the reaction of cyclopentadiene (**1**) and acrylonitrile (**6a**) show that the strain and solvation curves of both *endo* and *exo* approaches are almost identical, and the small differences in the strain curves are the underlying reason of the computed low selectivity (Figure 2A). In the case of

Table 1. Activation ($\Delta G^{\pm}$) and reaction (ΔG_{rxn}) Gibbs free energies [kcal mol^{-1}] of Diels-Alder cycloadditions depicted in Scheme 2 computed at M06-2X(PCM)/TZVP level. Thermal corrections were computed at 373.15 K. Theoretical and experimental *endo*:*exo* selectivities are also included.

Entry	Dienophile		$\Delta G^{\pm}$	ΔG_{rxn}	*endo*:*exo*	
					Theoretical	Experimental[a]
1	**6a**	*endo*	21.62	−16.65	53:47	55:45
2		*exo*	21.70	−16.63		
3	**6b**	*endo*	25.17	−13.18	11:88	16:84
4		*exo*	23.94	−13.45		
5	**7a**	*endo*	20.96	−15.35	74:26	70:30
6		*exo*	21.59	−15.05		
7	**7b**	*endo*	24.07	−12.33	33:68	32:68
8		*exo*	23.64	−11.99		

[a] Values taken from Ref. [20].

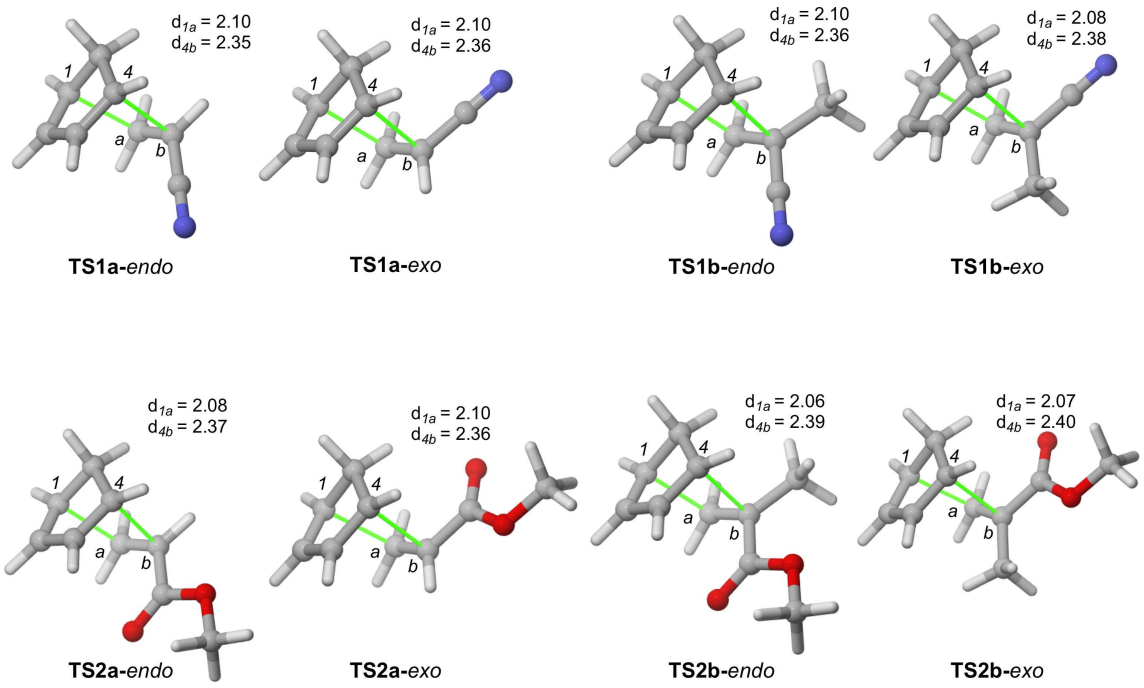

Figure 1. Main geometrical features of transition structures associated with the Diels–Alder cycloadditions depicted in Scheme 2 computed at the M06-2X (PCM)/TZVP level.

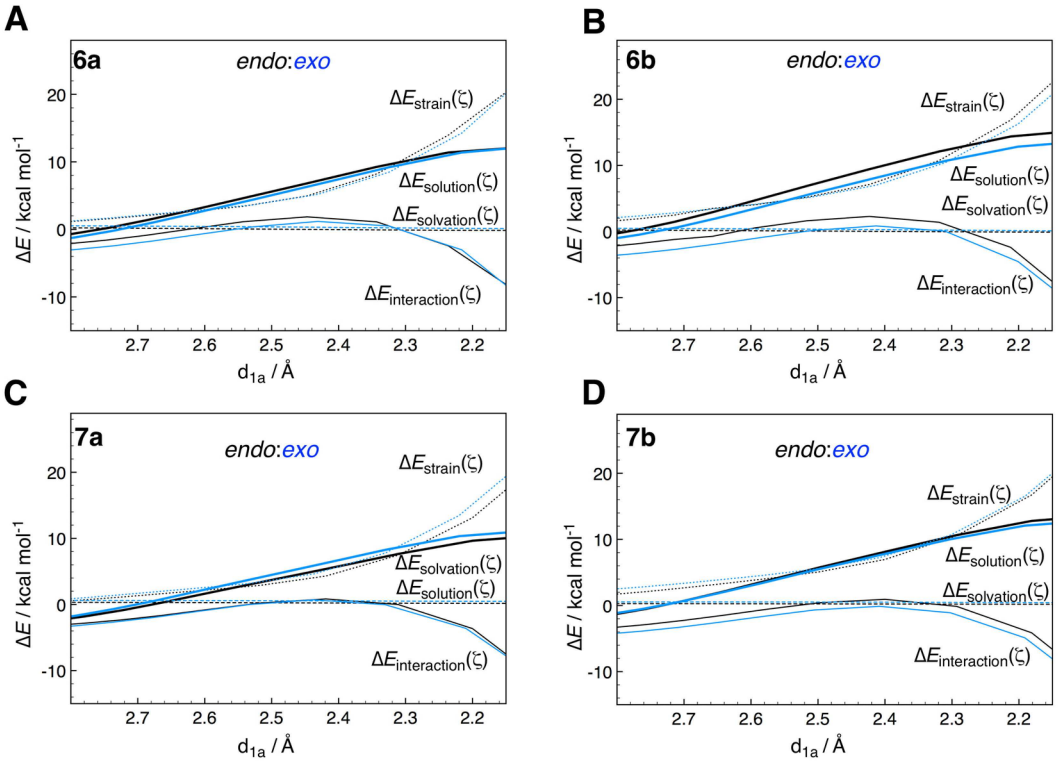

Figure 2. Comparative activation strain diagrams (ASDs) for the *endo* (black lines) and *exo* (blue lines) approaches of the Diels-Alder reaction of cyclopentadiene (**1**) with (A) **6a**, (B) **6b**, (C) **7a** or (D) **7b** as dienophiles along the reaction coordinate projected onto the forming carbon-carbon bond distance d_{1a}.

methacrylonitrile (**6b**), a higher stabilization in the *exo*-interaction curve is observed due to the presence of the α-methyl substituent. Decomposition of the interaction curve shows that it can be addressed to a lower Pauli repulsion

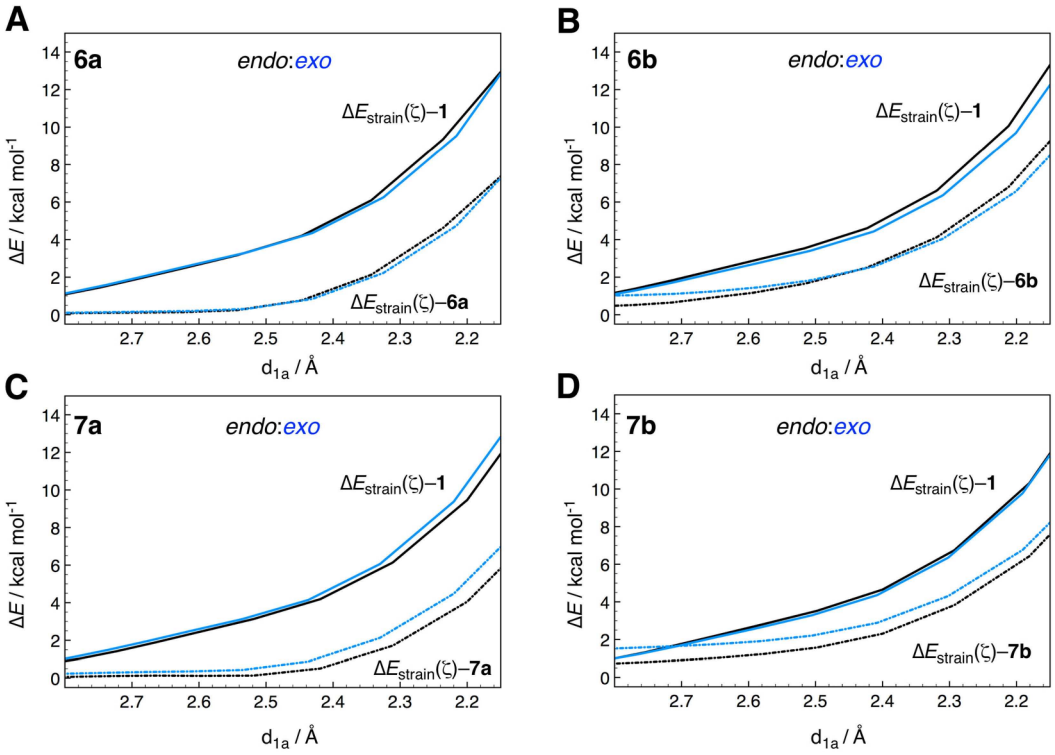

Figure 3. Decomposition of the strain energy in their fragments for the *endo* (black lines) and *exo* (blue lines) approaches of the Diels-Alder reaction of cyclopentadiene (**1**) with (A) **6a**, (B) **6b**, (C) **7a** or (D) **7b** as dienophiles.

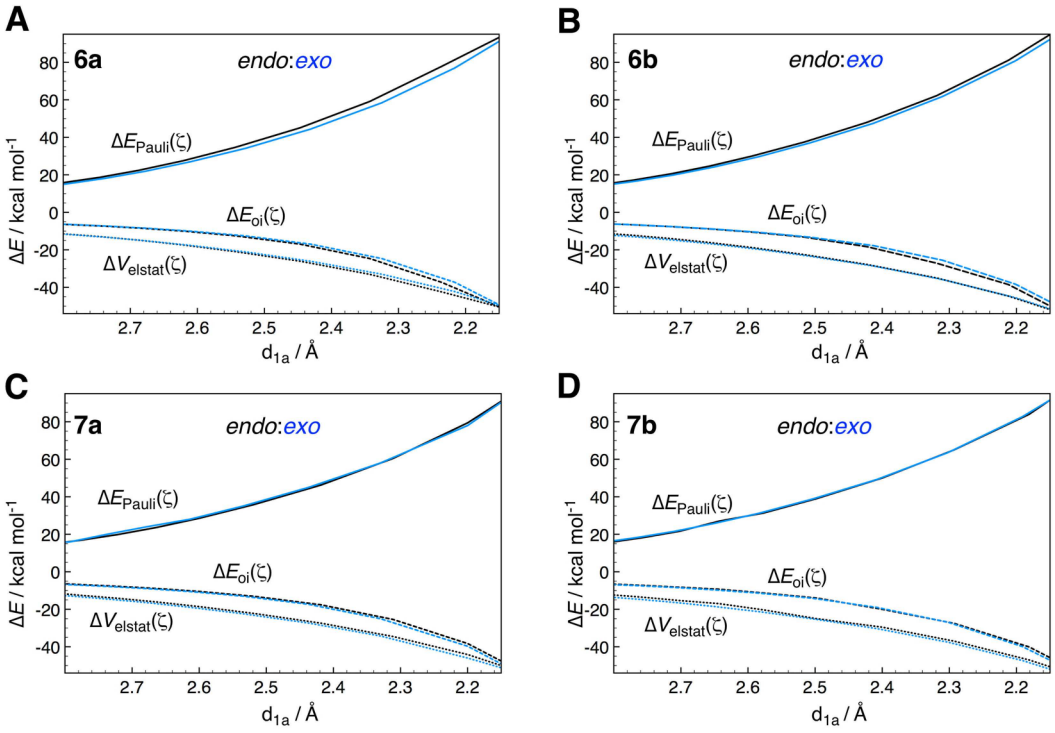

Figure 4. EDA analysis for the *endo* (black lines) and *exo* (blue lines) approaches of the Diels-Alder reaction of cyclopentadiene (**1**) with (A) **6a**, (B) **6b**, (C) **7a** or (D) **7b** as dienophiles computed at the M06-2X/TZVP level by using geometries optimized at M06-2X(PCM)/TZVP level.

instead of more stabilizing electrostatic or orbital interactions (Figure 4B). Moreover, at the beginning of the reaction, the strain curve of *exo* and *endo* approaches are similar, but in the proximities of the transition structure, there is an additional

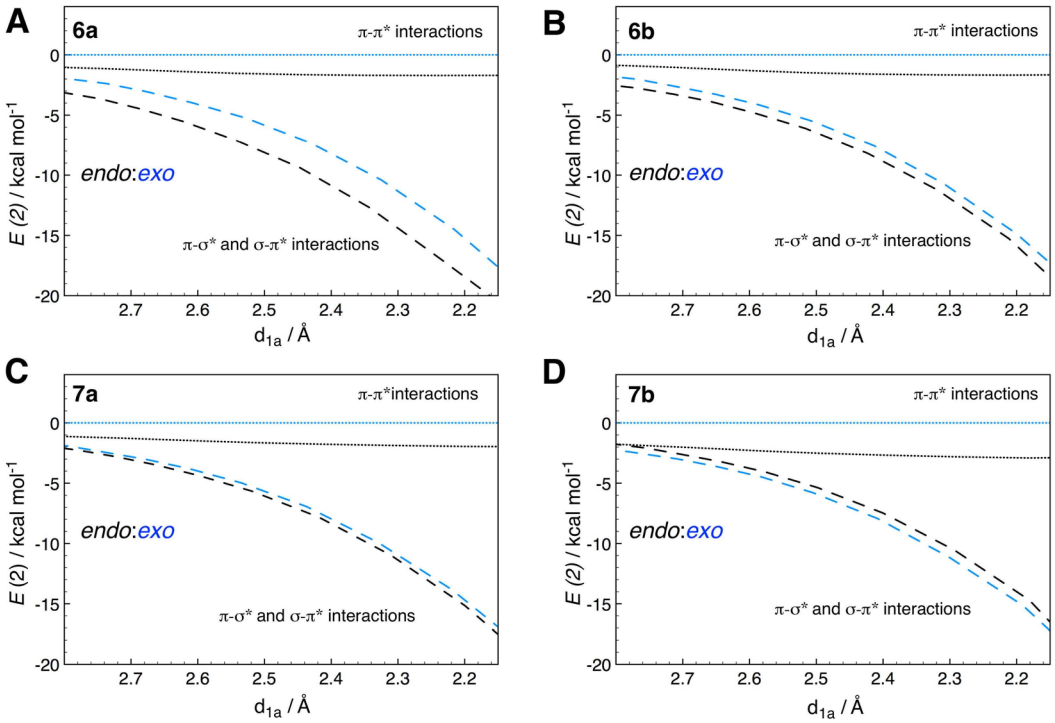

Figure 5. Comparative representation of second order perturbation energies (*E(2)*) between π–π* orbitals (dotted) or π–σ* + σ–π* orbitals (dashed) not directly involved in the carbon-carbon bond formation for the *endo* (black lines) and *exo* (blue lines) approaches of the Diels-Alder reaction of cyclopentadiene (**1**) with (A) **6a**, (B) **6b**, (C) **7a** or (D) **7b** as dienophiles. Negative signs are used to indicate that *E(2)* are stabilizing.

destabilization in the *endo* approach that makes the barrier to rise. Therefore, according to the computed ASM, this effect, together with the more stabilizing *exo* interaction curve, is the one responsible of the observed selectivity.

As far as acrylate derivatives are concerned, our results show a different scenario. In the reaction of cyclopentadiene (**1**) with methylacrylate (**7a**), the strain curve associated with the *endo* approach is more stable than the *exo* strain curve, being the interaction and solvation curves almost identical. That difference in the strain curves can be addressed to a higher deformation of both fragments (Figure 3C). Noticeably, the interaction curve associated with the *exo* approach is slightly more stabilizing in the proximity of the TSs, as consequence of subtle differences in the orbital interaction and Pauli repulsion curves (Figure 4C). Nevertheless, that higher interaction stabilization is incapable to overcome the strain penalty, thus, *endo* preference is observed. This result agrees whit the strain-based explanation for the *endo* selectivity in the reaction of cyclopentadiene (**1**) and maleic anhydride[22] (**2**) reaction proposed by Fernández and Bickelhaupt.[11]

In the case of methyl methacrylate (**7b**) as dienophile, the ASDs show a higher stabilization of the *exo*-interaction curve due to the presence of the α-methyl substituent, similar to methacrylonitrile (**6b**) case. However, our EDA calculations show that this higher stabilization is consequence of small differences in the electrostatic interactions[15] (Figure 4 D). Here, this higher interaction is capable to overcome the strain-penalty of the *exo* approach, thus prompting *exo*-cycloadduct formation.

In addition, the computed ASD show the relatively low relevance of solvation in the *endo*:*exo* selectivity of the selected Diels-Alder cycloadditions.

Next, we further analyzed the orbital interaction between reagents along the reaction coordinate ζ by means of NBO second order perturbation energy (Figure 5).[23] Within this localized orbital-based method, we split orbital interactions as: (a) primary orbital interactions, directly related to the formation of new C–C σ-bonds (not included in Figure 4); (b) secondary orbital interactions (classical SOI) as defined by Hoffmann and Woodward,[3] that is interaction between p orbitals not directly involved in the formation of new C–C σ-bonds (named as $\pi_{C-X-} > \pi^*_{C-X'}$ in Figures 6–9); and (c) hyperconjugative interactions: interactions between σ- and π-orbitals. These later interactions have been proven to be relevant in the observed selectivity of some chemical reactions.[18,24] Note that *E(2)* is somehow related to $\Delta E_{oi}(\zeta)$ but considering NBO localized orbitals instead of canonical Kohn-Sham ones.

With this analysis we try to shed light on the underlying reasons of the stabilization increase observed in the interaction curves as consequence of the presence of the methyl group in the dienophile despite not having p orbitals capable to interact with the diene.

The results obtained for the reaction of cyclopentadiene (**1**) and acrylonitrile (**6a**) show the existence of π–π stabilizing interactions that favor the *endo* approach that do not exist in the *exo* approach (Figure 6). These interactions correspond to the classical SOI and imply stabilization of the *endo* approach of ca. 2 kcal mol^{-1}. In addition, our analysis also point out the

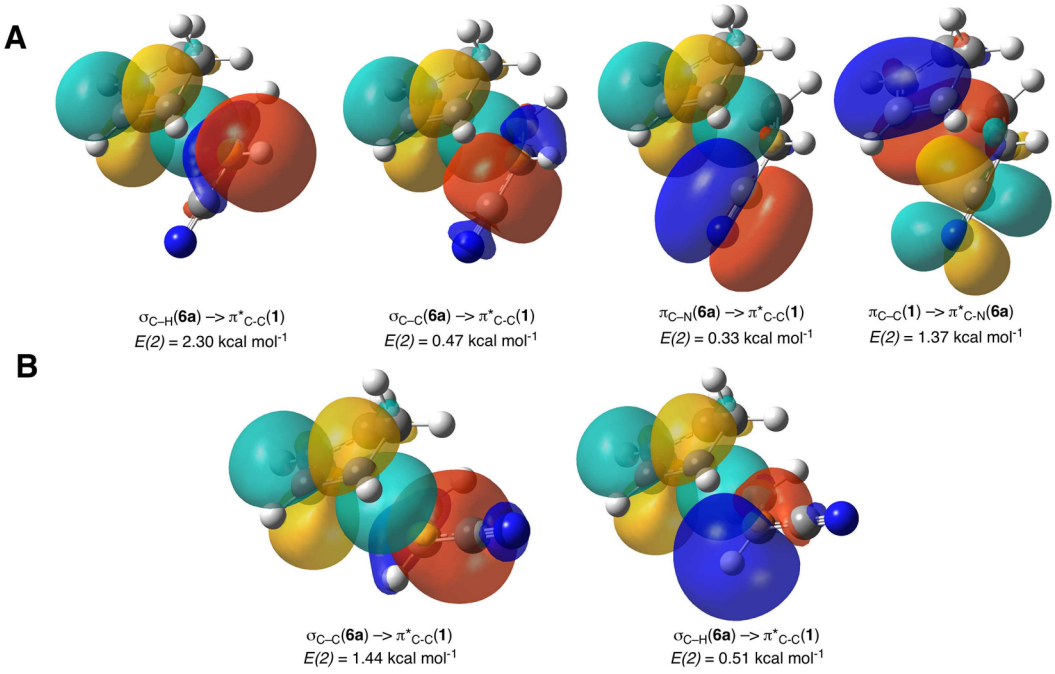

Figure 6. Representation of selected localized–orbital interactions not directly involved in the carbon-carbon bond formation in the (A) *endo* and (B) *exo* of transition structures associated with the Diels-Alder reaction of cyclopentadiene (**1**) with **6 a**. Red/blue and yellow/green surfaces represent occupied and virtual orbitals, respectively. Computed second order perturbation energies (*E(2)*) in the transition structure are included.

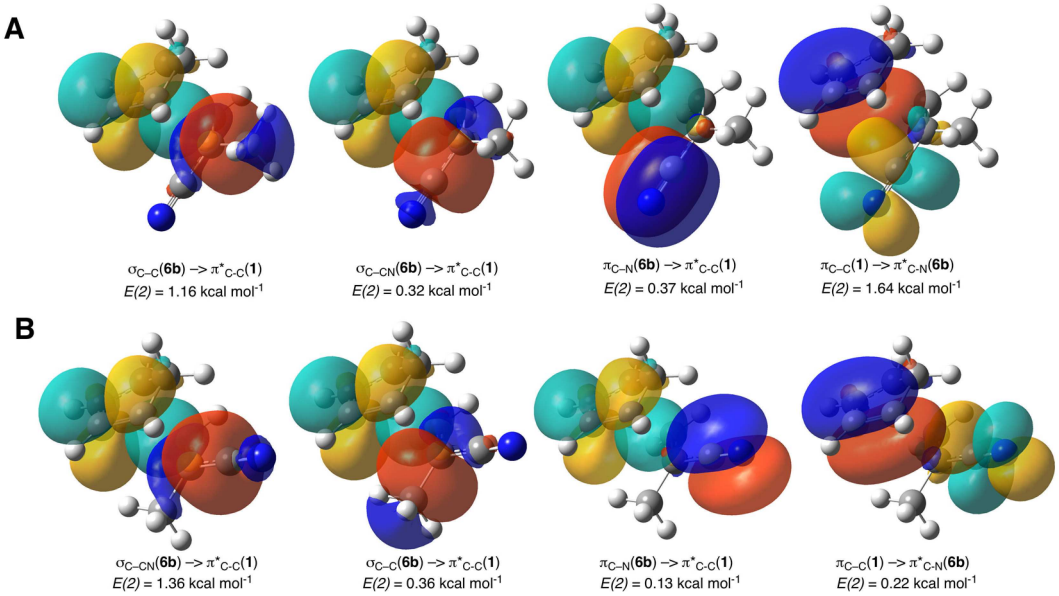

Figure 7. Representation of selected localized-orbital interactions not directly involved in the carbon-carbon bond formation in the (A) *endo* and (B) *exo* of transition structures associated with the Diels-Alder reaction of cyclopentadiene (**1**) with **6 b**. See the caption of Figure 6 for further details.

existence of relevant σ–π* interactions that also favors the *endo* approach. Moreover, C–H σ bond in outer position appears to be the optimal to interact with π^*_{C-C}(**1**) (*E(2)* = 2.30 kcal mol^{-1}). Nevertheless, the lower Pauli repulsion in the *exo* pathway (Figure 4A), factor not considered in this NBO analysis, compensates these SOI interactions, as reflected by the similar interactions curves obtained in the ASD (Figure 2A). The presence of the methyl group in the dienophile **6 b** implies a distortion in the geometry of the TS (vide supra). As a consequence both approaches present π–π stabilizing interactions, therefore, smaller stabilization of the *endo* approach by classical SOI is observed (only of 1.64 kcal mol^{-1}). In this case, the most relevant σ–π interactions are the ones involving π^*_{C-C} (**1**) and σ_{C-CN}(**6 b**) bonds, whose *E(2)* value is comparable to the SOI stabilization (1.36 kcal mol^{-1} for σ_{C-CN}(**6 b**)–> π^*_{C-C}(**1**) interaction and 1.64 kcal mol^{-1} for π_{C-C}(**1**)–>π^*_{C-N}(**6 b**) interaction).

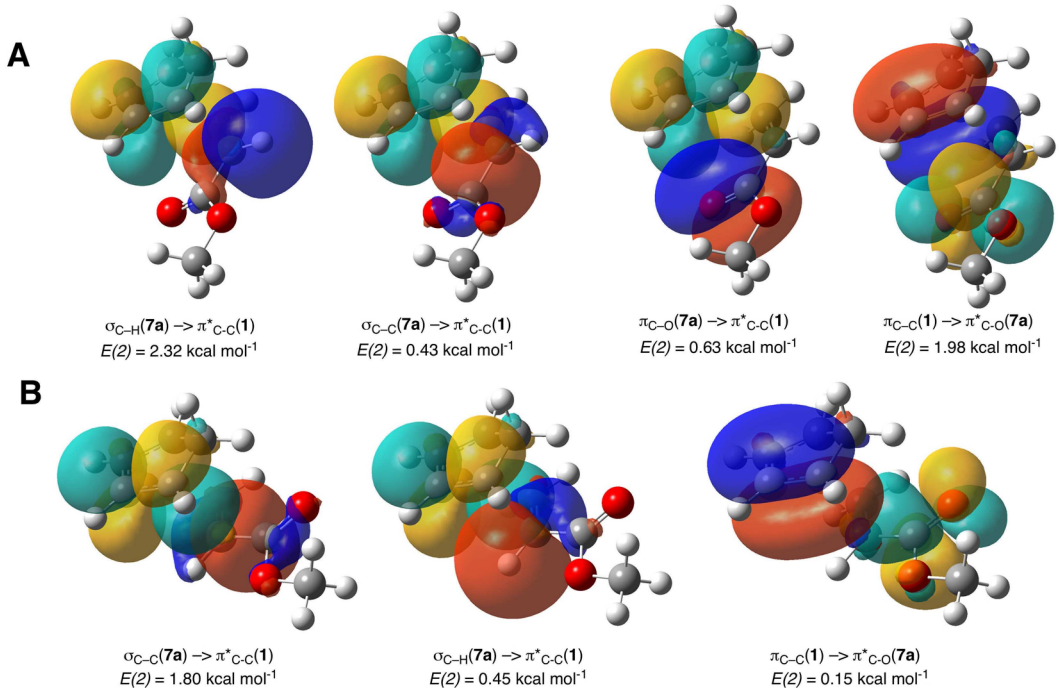

Figure 8. Representation of selected localized–orbital interactions not directly involved in the carbon-carbon bond formation in the (A) *endo* and (B) *exo* of transition structures associated with the Diels-Alder reaction of cyclopentadiene (**1**) with **7a**. See the caption of Figure 6 for further details.

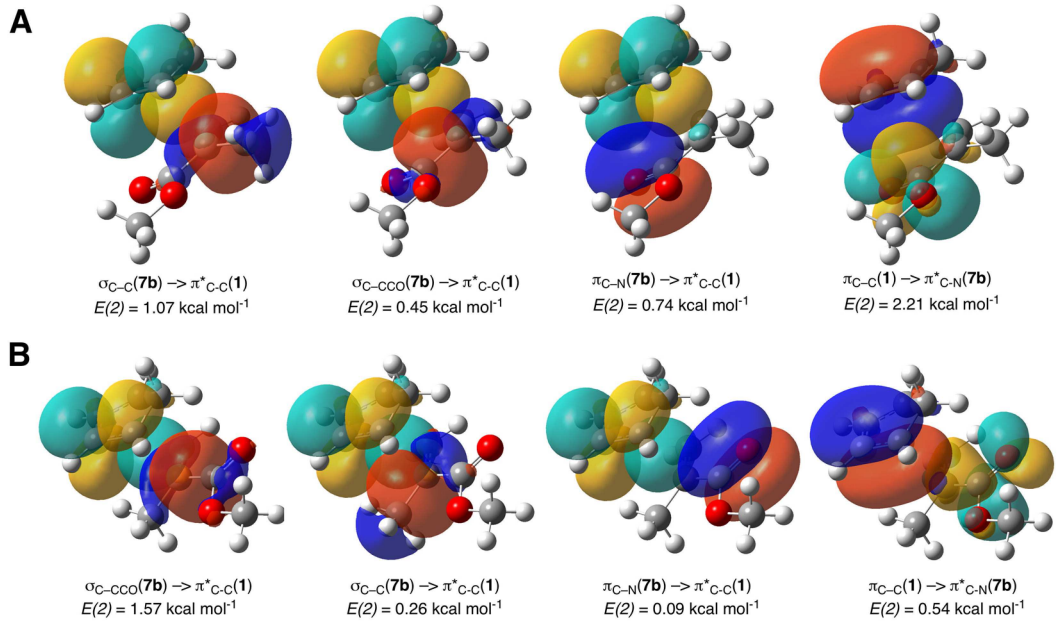

Figure 9. Representation of selected localized-orbital interactions not directly involved in the carbon-carbon bond formation in the (A) *endo* and (B) *exo* of transition structures associated with the Diels-Alder reaction of cyclopentadiene (**1**) with **7b**. See the caption of Figure 6 for further details.

Again, the outer position is the optimal one for that σ–π* interaction, thus favoring the *exo* approach instead. Those two factors (classical SOI and interaction with σ_{C-H}(**6a**) bond in outer position) that favored the *endo* approach for **6a** are less relevant in **6b**, therefore, NBO analysis indicates that *endo* approach is relatively less preferred for the latter (Figure 8; Figure 9).

Regarding acrylate derivatives, our *E(2)* results point out to a similar interpretation. In the case of **7a**, classical SOI strongly favors the *endo* approach, which is also favored by the optimal σ_{C-H}(**7a**)–> π^*_{C-C}(**1**) interaction in outer position. However, these factors are of low importance as shown in the ASD and EDA calculations, since both *endo* and *exo* interaction ($\Delta E_{int}(\zeta)$ in Figure 2C) and orbital interaction (ΔE_{oi} (ζ) in Figure 4C)

curves are almost identical and the *endo* selection relies on the different strain curve. On the other hand, in the case of methylated **7b**, SOI still favors the *endo* approach. However, σ–π* interactions strongly favor the *exo* approach (stripped blue line in Figure 5D). This is also reflected in a more stabilizing interaction curve (Figure 2D) that relies in a more stabilizing electrostatic interactions (Figure 4D), which favors *exo*-cycloadduct formation, despite the more energetic *exo* strain curve. Noticeably, in the reactions here analyzed, the SOI are not reflected in a more stabilizing *endo* orbital interaction curve, thus pointing out to the relatively low relevance of these particular orbital interactions in the selectivity of Diels-Alder cycloadditions.

3. Conclusions

Here, we have reported a detailed computational study of the Diels-Alder reaction of cyclopentadiene (**1**) with dienophiles **6**–**7a**,**b** at M06-2X(PCM)/TZVP level of theory in order to understand the excellent *exo*-selectivities observed experimentally due the presence of the α-methyl substituent. Further analysis of the reaction coordinate by means of activation strain model of chemical reactivity (ASM-distortion interaction model) and NBO second order perturbation energy show that Diels-Alder *endo*:*exo* selectivities are strongly dependent of the system considered, and no general trend can be extrapolated from model (unsubstituted) reactions. In the studied reactions, introduction of a methyl group implies an increase of the reaction barrier in both approaches. That *exo* preference observed in methyl-substituted systems can be addressed to the existence of higher stabilizing interactions as consequence of lower Pauli repulsion or higher electrostatic interactions rather than more stabilizing orbital interactions. In addition, secondary orbital interactions (classical SOI) seem to be of relatively low relevance in the interaction curves, and therefore, in the selectivity.

Computational Details

Theoretical calculations have been carried out within the DFT framework.[25] Reaction profiles and NBO analysis have been carried out at the M06-2X(PCM)/TZVP level by using the GAUSSIAN 16[26] suite of programs. Energy Decomposition Analysis (EDA) have been carried out at M06-2X/TZVP level (using previously optimized geometries) with ADF2017[27] program. This highly parameterized method, well suited for the treatment of nonbonding interactions and dispersion forces,[28] was chosen after an initial benchmark study (see Supporting Information). Thermal Gibbs corrections were computed at the same level, at 373.15 K, and were not scaled. Solvent effects were estimated by the polarization continuum model[29] (PCM) method within the self-consistent reaction field (SCRF) approach.[30] All SCRF-PCM calculations were performed using benzene (ε = 2.2706) as model solvent.

All the stationary points were characterized by harmonic vibrational analysis. Local minima showed positive definite Hessians. Fully optimized transition structures showed only one imaginary frequency associated with nuclear motion along the chemical transformation under study. Reaction paths were checked by intrinsic reaction coordinates (IRC) calculations.

Second order perturbation energies $E(2)$ were computed according to the NBO[9] method implemented in Gaussian16 following Equation (1):

$$E(2) = -n_{\phi}\frac{\langle\phi|F|\phi^{*}\rangle^{2}}{\varepsilon_{\phi}{}^{*} - \varepsilon_{\phi}} \quad (1)$$

where $<\varphi|F|\varphi^{*}>$ is the Fock matrix element between the orbitals φ and φ^{*}, ε_{φ} and $\varepsilon_{\varphi^{*}}$ are the energies of φ and φ^{*} orbitals and n_{φ} is the population of the donor orbital. Localized molecular orbitals were also computed with the NBO method.

The computed reaction profiles were analyzed using the activation strain (ASM) – distortion/interaction model[12] developed by Bickelhaupt – Houk, respectively, modified to include solvation effects.[31] Within this framework, the solution-phase energy profile $\Delta E_{\text{solution}}(\zeta)$ is decomposed along the reaction coordinate ζ into the energy of the solute $\Delta E_{\text{solute}}(\zeta)$, the reaction system in vacuum but with its geometry in solution, plus the solvation energy $\Delta E_{\text{solvation}}(\zeta)$ [Eq. (2)]:

$$\Delta E_{\text{solution}}(\zeta) = \Delta E_{\text{solute}}(\zeta) + \Delta E_{\text{solvation}}(\zeta) \quad (2)$$

In the present work, the reaction coordinate ζ is projected onto the carbon-carbon bond distance of cyclopentadiene (**1**) and the corresponding dienophile. In all cases, the shortest C–C distance (d_{1a}) was chosen as reaction coordinate ζ. $\Delta E_{\text{solvation}}(\zeta)$ accounts for both the interaction of the solute with the solvent and the cavitation energy.

The solute energy $\Delta E_{\text{solute}}(\zeta)$ is further decomposed as [Eq. (3)]:

$$\Delta E_{\text{solute}}(\zeta) = \Delta E_{\text{strain}}(\zeta) + \Delta E_{\text{int}}(\zeta) \quad (3)$$

where $\Delta E_{\text{strain}}(\zeta)$ and $\Delta E_{\text{int}}(\zeta)$ correspond to the strain and interaction energy, respectively. The strain energy is associated with the required energy to deform the reactants from their equilibrium geometry to the geometry they adopt along ζ. This term depends on the rigidity of the reactants and, in general, is positive (destabilizing) giving rise to the occurrence of the reaction barrier. On the other hand, the interaction term $\Delta E_{\text{int}}(\zeta)$ depends on the electronic structure of the reagents and on how they approach each other. $\Delta E_{\text{int}}(\zeta)$ can be further analyzed within Kohn-Sham MO conceptual framework[13] according to the Energy Decomposition Analysis (EDA)[13] as Equation (4):

$$\Delta E_{\text{int}}(\zeta) = \Delta V_{\text{elstat}}(\zeta) + \Delta E_{\text{Pauli}}(\zeta) + \Delta E_{\text{oi}}(\zeta) \quad (4)$$

where $\Delta V_{\text{elstat}}(\zeta)$ corresponds to the classical Coulombic interaction between the charge distribution of the reactants, $\Delta E_{\text{Pauli}}(\zeta)$ correspond to the Pauli repulsions between occupied orbitals of the fragments and is responsible for steric repulsion. The orbital interaction term $\Delta E_{\text{oi}}(\zeta)$ includes the charge transfer interactions and polarization. Note that both primary and secondary orbital interactions are included within this latter term.

Endo:*exo* selectivities have been computed by using the Eyring-Polanyi equation[32] from the previously computed Gibbs free activation energies ($\otimes G^{\pm}$), applying Curtin-Hammet kinetics (the product ratio depends on energy differences of the corresponding TSs).

Supporting Information

Initial level of theory benchmark, NBO second perturbation energies, cartesian coordinates, energies and number of imaginary points of all local minima and transition structures discussed in this work.

Acknowledgements

This work was supported by funding provided by the Spanish Ministry of Economy and Competitiveness (MINECO CTQ2013-45415P) and the Gobierno Vasco-Eusko Jaurlaritza (grant IT673-13). O.L. gratefully acknowledges the UPV/EHU for her postdoctoral grant. SGI-IZO-SGIker (UPV/EHU) and DIPC are acknowledged for generous allocation of computational resources.

Conflict of Interest

The authors declare no conflict of interest.

Keywords: activation strain model · cycloaddition · density functional calculations · Diels-Alder reactions · second order perturbation energy · selectivity

[1] a) S. Lobayashi, K. A. Jorgensen, Eds. *Cycloaddition Reactions in Organic Syntehsis*; Willey-VCH: Weinheim, **2001**; b) S. M. Bachrach *Computational Organic Chemistry*; John Willey & Sons Inc.: Hoboken, New Jersey, **2007**.
[2] K . Alder, G. Stein *Justus Liebigs Ann. Chem.* **1934**, *514*, 1–33.
[3] a) R. Hoffmann, R. B. Woodward *J. Am. Chem. Soc.* **1965**, *87*,4388–4389; b) B. R. Woodward, R. Hoffmann *The Conservation of Orbital Symmetry*; Academic Press: New York, **1969**.
[4] a) C. S. Wannere, A. Paul, R. Herges, K. N. Houk, H. F. Schaefer III, P. v. R. Schleyer *J. Comp- Chem.* **2007**, *28*, 344–361; b) I. Fleming *Frontier Orbitals and Organic Chemical Reactions*; Wiley: New York, **1976**.
[5] a) J. I. García, J. A. Mayoral, L. Salvatella *Acc. Chem. Res.* **2000**, *33*, 658–664.; b) I. Fleming *Pericyclic reaction*; Oxford University Press: Oxford, **1999**, pp. 49; c) J. D. Xidos, T. L. Gosse, E. D. Burke, R. A. Poirier, J. D. Burnell, *J. Am. Chem. Soc.* **2001**, *123*, 5482–5488.
[6] A. Arrieta, F. P. Cossío, B. Lecea *J. Org. Chem.* **2001**, *66*, 6178–6180.
[7] L. M. Stephenson, D. E. Smith, S. P. Current *J. Org. Chem.* **1982**, *47*, 4170–4171.
[8] a) G. Klopman *J. Am. Chem. Soc.* **1968**, *90*, 223–234; b) L. Salem *J. Am. Chem. Soc.* **1968**, *90*, 543–552.
[9] a) F. Weinhold, C. R. Landis *Discovering Chemistry with Natural Bond Orbitals*; John Wiley & Sons. Inc.: Hoboken, New Yersey, **2012**; b) F. Weinhold, C. R. Landis *Valence and Bonding, a Natural Bond Orbital Donor-Acceptor Perspective*; Cambridge Univ. Press.: Cambridge, UK, **2005**.
[10] L. Rulisek, P. Sebek, Z. Havlas, R. Hrabal, P. Capek, A. Svatos *J. Org. Chem.* **2005**, *70*, 6295–6302.
[11] a) I. Fernández, F. M. Bickelhaupt *J. Comput. Chem.* **2014**, *35*, 371–376; b) I. Fernández, F. M. Bickelhaupt *Chem. Asian J.* **2016**, *11*, 3297–3304.
[12] a) F. M. Bickelhaupt, K. N. Houk *Angew. Chem.* **2017**, *129*, 10204–10221; *Angew. Chem. Int. Ed.* **2017**, *56*, 100070–10086; b) L. P. Wolters, F. M. Bickelhaupt *WIREs Comput. Mol. Sci.* **2015**, *5*, 324–343; c) I. Fernández, F. M. Bickelhaupt *Chem. Soc. Rev.* **2014**, *43*, 4953–4967; d) D. H. Ess, K. N. Houk *J. Am. Chem. Soc.* **2007**, *129*, 10646–10647; e) F. M. Bickelhaupt *J. Comput. Chem.* **1999**, *20*, 114–128.
[13] a) F. M. Bickelhaupt, E. J. Baerends *Reviews in Computational Chemistry Vol. 15*; K. B. Lipkowitz, D. B. Boyd Eds.; Wiley-VHC: New York, **2000**, pp. 1–86; b) M. Lein, G. Frenking *Theory and Applications of Computational Chemistry. The First 40 years*; C. E. Dykstra, G. Frenking, K. S. Kim, G. E. Scuseria, Eds.; Elsevier: Amsterdam, **2005**.
[14] Note that, by definition, SOI are included into the orbital interaction term of ASD.
[15] K. Sakata, H. Fujimoto *Eur. J. Org. Chem.* **2016**, 4275–4278.
[16] Y. Qiu *J. Phys. Org. Chem.* **2015**, *28*, 370–376.
[17] a) B. J. Levandowski, K. N. Houk *J. Am. Chem. Soc.* **2016**, *138*, 16731–16736; b) B. J. Levandowski, T. A. Hamlin, R. C. Helgeson, F. M. Bickelhaupt, K. N. Houk *J. Org. Chem.* **2018**, *83*, 3164–3170.
[18] B. J. Levandowski, L. Zou, K. N. Houk *J. Comput. Chem.* **2016**, *37*, 117–123.
[19] a) J. G. Martin, R. K. Hill *Chem. Rev.* **1961**, *61*, 537–562; b) D. L. Boger *Chem. Rev.* **1986**, *86*, 781–794; c) N. Nishiwaki Ed. *Methods and Applications of Cycloadditon Reactions in Organic Syntheses*; Wiley & Sons, Inc., Hoboken, New Yersey, **2014**; d) V. Froidevaux, M. Borne, E. Laborbe, R. Auvergne, A. Gandini, B. Boutevin *RSC Adv.* **2015**, *5*, 37742–37754; e) S. D. Tsai, R. A. Register *Macromol. Chem. Phys.* **2018**, *219*, 1800059.
[20] a) Y. Kobuke, T. Fueno, J. Furukawa *J. Am. Chem. Soc.* **1970**, *92*, 6548–6553; b) Y. Kobuke, T. Sugimoto, J. Furukawa, T. Fueno *J. Am. Chem. Soc.* **1972**, *94*, 3633–3635.
[21] a) F. K. Brown, K. N. Houk *Tetrahedron Lett.* **1985**, *26*, 2297–2300; b) B. R. Beno, K. N. Houk, D. A. Singleton *J. Am. Chem. Soc.* **1996**, *118*, 9984–9985; c) D. A. Singleton, B. E. Schulmeier, C. Hang, A. A. Thomas, S.-W. Leung, S. R. Merrigan *Tetrahedron* **2001**, *57*, 5149–5160; d) M. Linder, T. Brink *Phys. Chem. Chem. Phys.* **2013**, *15*, 5108–5114.
[22] This is consequence of structural similarities between **7 a–b** and **2**.
[23] See the Supporting Information for the complete set of computed second order perturbation energies.
[24] I. A. Alabugin, K. M. Gilmore, P. W. Peterson *WIREs Comput. Mol. Sci.* **2011**, *1*, 109–141.
[25] R. G. Parr, W. Yang, *Density-Functional Theory of Atoms and Molecules*, Oxford, New York, **1989**.
[26] Gaussian16, Revision B.01, M. J. Frisch et al., Gaussian Inc., Wallingford CT, **2016** (full reference in the Supporting Information).
[27] S. C. M. ADF2017.110 Theoretical Chemistry, Vrije Universiteit: Amsterdam, **2017** (see www.scm.com).
[28] a) Y. Zhao, D. G. Truhlar, *Acc. Chem. Res.* **2008**, *41*, 157–167; b) Y. Zhao, D. G. Truhlar, *Theor. Chem. Acc.* **2008**, *120*, 215–241.
[29] R. Cammi, B. Mennucci, J. Tomasi, *J. Phys. Chem. A* **2000**, *104*, 5631–5637.
[30] J. Tomasi, B. Mennucci, R. Cammi, *R. Chem. Rev.* **2005**, *105*, 2999–3093.
[31] a) J. Z. A. Laloo, L. Rhyman, P. Ramasami, F. M. Bickelhaupt, A. de Cózar, *Chem. Eur. J.* **2016**, *22*, 4431–4439.; b) J. Z. A. Laloo, L. Rhyman, O. Larrañaga, P. Ramasami, F. M. Bickelhaupt, A. de Cózar, *Chem. Asian J.* **2018**, *13*, 1138–1147.
[32] H. Eyring, M. Polanyi, *Z. Phys. Chem. B* **1931**, *12*, 279–311.